Defect-Driven topology optimization for fatigue design of additive manufacturing structures: Application on a real industrial aerospace component

Defect-Driven Topology Optimization for fatigue design of Additive Manufacturing structures: Application on a real industrial aerospace component

C. Boursier Niutta[a*], A. Tridello[a], G. Barletta[c], N. Gallo[c], A. Baroni[c], F. Berto[d], D.S. Paolino[a,b]

[a]*Department of Mechanical and Aerospace Engineering, Politecnico di Torino, 10129 Turin, Italy*
[b]*IMAST S.c.ar.l.—Technological District on Engineering of Polymeric and Composite Materials and Structures, 80133 Napoli, Italy*
[c]*Aerostructures Division, Leonardo Spa, 74023 Taranto, Italy*
[d]*Department of Mechanical and Industrial Engineering, Norwegian University of Science and Technology (NTNU), Trondheim, Norway*
[*]Corresponding author: carlo.boursier@polito.it

Keywords: Topology Optimization, Fatigue, Defect Population, Additive Manufacturing

Abstract

In this paper, a generalized formulation of defect-driven topology optimization (TO) for fatigue design, named *TopFat*, is proposed, where the first principal stress, that causes the crack propagation, is limited in accordance with the defect size distribution of the additive manufacturing (AM) process. As the largest defect depends on the final volume of the component, which changes according to the topology, an iterative procedure is adopted to avoid volume constraints in the optimization problem. The procedure is applied to an actual aerospace bracket component and its strength and limitations are discussed in comparison with the TO formulations presented in the literature. Results show that considering the defect population significantly affects the final topology, while leading to a feasible optimum. Further, even though the computational time increases, an additional 15% of mass saving is achieved by adopting the proposed iterative procedure with respect to a volume constraint-based formulation of *TopFat*.

Nomenclature

AM: Additive Manufacturing
TO: Topology Optimization
FE: Finite Element
C: Compliance of the component
$\bar{\rho} = \{\rho_1, \rho_2, \dots, \rho_{N_e}\}$: Relative density of the N_e elements
V: Volume of the component
V_0: Initial volume of the component
V_{opt}: Optimal volume to obtain at the end of the TO
s_{eq}: Equivalent stress computed through some proper criterion, e.g., the Von Mises Criterion.
s_{adm}: Admissible stress, e.g. the yield limit of the material $R_{p0.2}$ or the ultimate strength R_m
s_1: First principal stress
s_{max}: Maximum allowable first principal stress
$\bar{\bar{K}}$: Stiffness matrix
$\bar{u}$: Displacement vector
$\bar{F}$: External force vector

s_l: Fatigue limit
HV: Vickers hardness
R: Stress ratio, i.e., the ratio between the minimum s_{min} and the maximum s_{max} stress in the load cycle
C_1: Constant coefficient depending on the defect location
$\sqrt{a_c}$: Critical defect size
LEVD: Largest Extreme Value Distribution
$\sqrt{a}_{c,n}$: The largest critical defect expected in a volume V_n equal to $V_n = n \cdot V_0$
V_{ref}: Reference volume
$\mu_{\sqrt{a}}$: Location parameter of the LEVD
$\sigma_{\sqrt{a}}$: Scale parameter of the LEVD distribution
F: Probability of the defect size of interest
V_{90}: Volume above the 90% of the maximum applied stress
HIP: Hot isostatic pressure
E: Young's modulus
ν: Poisson ratio

1. Introduction

Thanks to the continuous improvements in additive manufacturing (AM), topology optimization (TO) has become a feasible tool for the design of mechanical components in industrial applications. Examples of topology-optimized and additively manufactured components are nowadays more and more common in aerospace applications [1–3]. AM allows creating very complex and convoluted shapes [4,5], as well as complex features such as lattice structures and metamaterial cells [6–8]. In combination with TO algorithms, the best material distribution, i.e., the minimum mass for the required mechanical performances, can be concretely achieved, leading to effectively improved components [9–11]. However, it is well recognized that additively manufactured components are characterized by a significant presence of defects which affect in turn their mechanical performance. AM processes produce final parts affected by a non-negligible defect population, even if optimised process parameters are set [12–15]. According to [16], the AM defects can be generally classified as: (i) pores and clusters of pores, (ii) lack of fusion, (iii) irregular surface or subsurface defects and (iv) microstructural defects, i.e., microstructural discontinuities. These defects are almost always present in AM final part, and, even if are characterized by different types and morphologies, they all can be critical for the mechanical performance of the component [16]. The presence of such defects affects both the static strength and the fatigue limit of the final component.

In particular, regarding the fatigue response, the experimental activity has shown that the fatigue strength is inversely proportional to the size of the defect, which is the most influencing parameter for the fatigue response, together with the location of the defect [12,17–20]. On the contrary, the differences in the morphology can be neglected since the shape of the defect usually rounds under the first loading cycles [20].

In this framework, while a reduced strength can be considered in the design process for static loading conditions, the design of AM parts through TO under fatigue loads is still addressed through inefficient methodologies, as the stress limit mainly depends on the size and the location of the defects.

In practical applications, the influence of the defects is generally considered after the component has been manufactured [21,22]. Figure 1 shows a representative flowchart that is usually followed for the design of AM components subjected to fatigue loads during their in-service life.

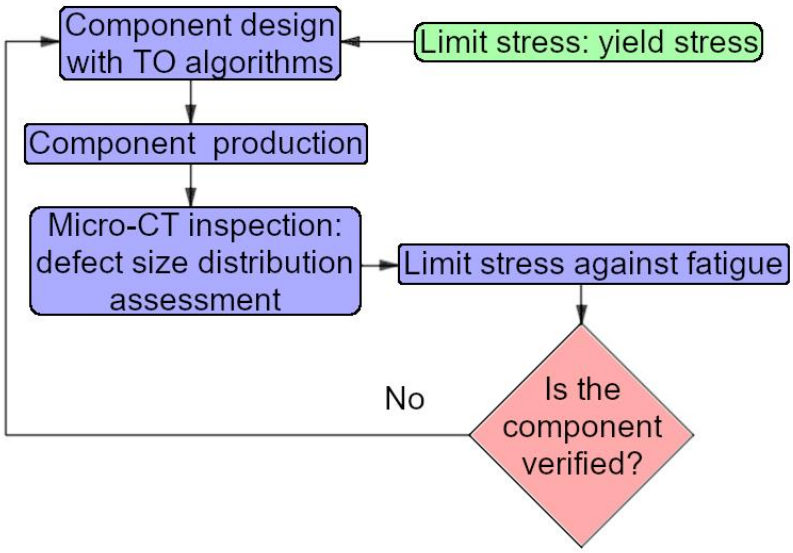

Figure 1. Component design with topology optimization algorithm and defect assessment with micro-CT inspection.

The topology optimization is carried out by minimizing the mass of the component while setting the quasi-static material properties as the critical limits, e.g., the yield stress or the ultimate tensile strength.

Thereafter the component is produced and finally a micro-CT analysis is carried out to assess the defect population within the material volume. Given the defect population in terms of size, morphology and location, the structural integrity of the component can be verified: for example, given the largest defect or the location and the distribution of the defects within the component volume, the limit stress can be computed, for example with the Murakami approach [23], and compared with the stress assessed through Finite Element (FE) analysis. However, if the applied stress at specific defect locations is larger than the limit stress, no further modifications are possible and the component has to be redesigned and produced again, thus affecting the manufacturing costs. This design approach allows to directly verify if the component can withstand the applied fatigue loads and is, therefore, the safest, since not based on an assumed defect size distribution. On the other hand, depending on the defect size distribution, the structural integrity of the component can be verified only at the end of the design process.

Another approach that can be followed is shown in the flowchart in Figure 2.

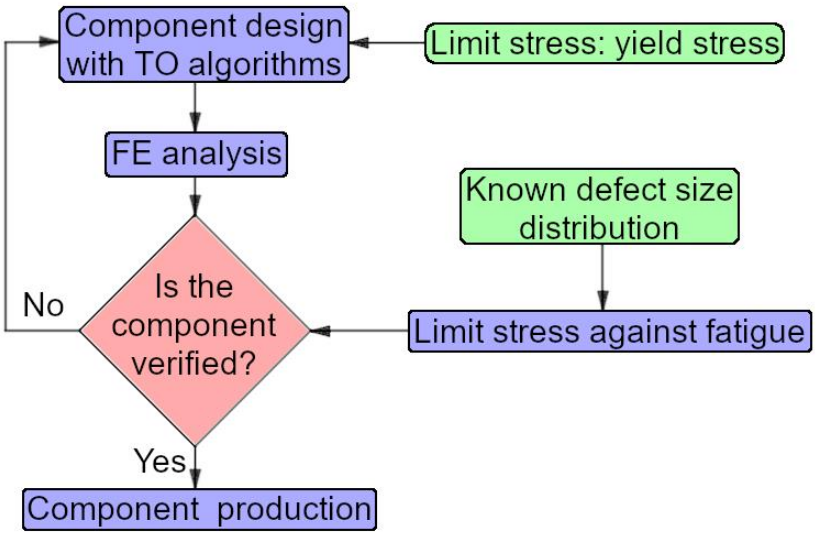

Figure 2. Component design with topology optimization algorithm and analysis of the influence of defects after the topology optimization process.

This approach involves the design of the component through TO algorithms, followed by a FE analysis on the optimized component. The dependency of the fatigue response on the defect size is here accounted for the validation of the optimal topology. In particular, the defect size population can be modeled through the extreme value distribution [24], which has been successfully applied also to AM specimens [25]. Romano et al. [22] have recently compared the probability distribution of defect size based on the μ-CT data with that based on the optical microscopy data of AlSi10Mg specimens manufactured through three different processes. Results have shown that both μ-CT and optical microscopy are able to predict the variation of defect size distribution between the three processes. Tridello et al. [12] have used the Largest Extreme Value Distribution (LEVD) to investigate the dependency of the VHCF response of AlSi10Mg specimens on the defect size.

The component structural integrity is thus verified by comparing the maximum first principal stress within the optimized morphology with the allowable stress computed by considering the defect size distribution. For example, according to the Murakami approach [20,23], once a proper distribution for the defect size population is assumed and identified, the corresponding fatigue limit can be calculated and adopted for the design verification. If the maximum stress is above the limit value, the component must necessarily be redesigned with a second TO. In this case, the second design can be carried out by reducing the limit stress in the TO, with a trial-and-error time-consuming scheme. With this second approach, the influence of defects on the fatigue strength is verified before the specimen is produced, but with a trial-and-error approach, the design process is not efficient. A probabilistic approach can be also employed [26], providing important indications on the reliability of the part, and further modifications can be made by the designer to limit the stress in critical regions. However, these modifications depend on the designer's choice. It must be also noted that setting the free of defects fatigue limit as the allowable stress during the TO may also be unsafe, since the defect-free fatigue limit represent an upper limit decreasing as the defect size increases (according to the Kitagawa-Takahashi diagram).

In this paper, the design of topology-optimized parts subjected to both static and fatigue loads is addressed. A generalized formulation of a recently proposed methodology, named *TopFat*, for the design of AM parts through TO is proposed and applied to a real-world aerospace case. In particular, the paper is organized as follows: in Section 2, the *TopFat* methodology is presented and its

implementation into the TO framework of the commercial software *Hypermesh* is described. In Section 3, the methodology is shown on an aerospace bracket which connects the hatboxes to the structural beams of the aircraft fuselage. The structural-mechanical problem is presented and addressed with the *TopFat* scheme. In order to show the strength and the possible limitations of the proposed methodology, the results of the TO are compared to those obtained with the approaches presented in the literature and described above. In particular, the three optimizations are performed in addition: in the first, the fatigue limit is not considered, i.e., the bracket is optimized only with respect to the static conditions, as described in the flowchart of Figure 2; in the second, a defect-free maximum allowable stress is considered for the fatigue limit; in the third, a TO with volume constraint, as in the original formulation of the *TopFat* algorithm, is considered. Finally, conclusions are given.

2. *TopFat* Methodology

In this Section, the methodology developed for generalizing the *TopFat* methodology is described. In Section 2.1, the original formulation of the *TopFat* methodology is presented [27], highlighting its strength and limitations. In Section 2.2 the general procedure developed for implementing the *TopFat* methodology without volume constraints is reported in detail.

2.1 *TopFat* methodology with volume constraints

The so-called *TopFat* methodology has been originally proposed by the Authors in [27] to prevent fatigue failures from manufacturing defects in components designed through TO algorithms. Accordingly, this methodology is particularly appropriate for AM parts, that are generally designed with TO algorithms and are prone to fatigue failures at stress smaller than that critical for components produced with traditional processes, due to the presence of larger manufacturing defects. Indeed, manufacturing defects are preferential sites for crack formation and propagation up to the final failure. Therefore, a stress limit that models the influence of defects must be considered when AM components are designed, in order to guarantee their structural integrity during the in-service life.

The *TopFat* methodology permits overcoming the weaknesses of the two main approaches described above, thus integrating the design against fatigue failures from defects within the TO framework [28]. The optimization problem is formulated in order to constrain the first principal stress, which is responsible for the crack propagation from defects [26]. In particular, the first principal stress is limited by taking into account the defect size directly during the TO process. In its original formulation, the *TopFat* optimization problem has been written as [28]:

$$\begin{aligned} & \min_{\bar{\rho}} \; C(\bar{\rho}) \\ \text{such that} \quad & \frac{V}{V_{opt}} - 1 \leq 0 \\ & \frac{s_{eq}}{s_{adm}} - 1 \leq 0 \\ & \frac{s_1}{s_{max}} - 1 \leq 0 \\ & \rho_{inf} \leq \rho_e \leq 1 \\ \text{where} \quad & \bar{\rho} = \{\rho_1, \rho_2, \dots, \rho_{N_e}\} \end{aligned} \tag{1}$$

governed by $\bar{\bar{K}}(\bar{\rho})\bar{u} = \bar{F}$

where $C(\bar{\rho})$ is the global compliance of the component, $\bar{\rho} = \{\rho_1, \rho_2, \dots, \rho_{N_e}\}$ the vector of the design variables, i.e., the relative densities of the N_e elements, V the actual volume of the component, V_{opt} the final volume to obtain, s_{eq} the equivalent stress at each element of the FE analysis computed through some proper criterion, s_{adm} the admissible stress, e.g. the yield stress, s_1 is the first principal stress of each element and s_{max} is the maximum allowable principal stress, $\bar{\bar{K}}(\bar{\rho})$ the stiffness matrix which depends on the relative densities $\bar{\rho}$ (e.g., as in SIMP approach), $\bar{u}$ the displacement vector and $\bar{F}$ the external force vector. In topology optimization algorithms, the lower limit of the densities ρ_{inf} is usually set in the range $[0.0001, 0.001]$ in order to avoid numerical instabilities.

According to [23], the fatigue limit, i.e., the threshold for crack propagation, is

$$s_l = \frac{C_1 \cdot (HV + 120)}{\left(\sqrt{a_c}\right)^{\frac{1}{6}}} \cdot \left(\frac{1 - R}{2}\right)^{0.226 + HV \cdot 10^{-4}} \quad (2)$$

where HV is the Vickers hardness, R the stress ratio, defined as the ratio between the minimum s_{min} and the maximum s_{max} stress in the load cycle, C_1 is a constant coefficient depending on the defect location and $\sqrt{a_c}$ is the critical defect size. To model the probabilistic increment of the defect size with the loaded volume, the defect size is assumed as a random variable following the LEVD. By exploiting the properties of the LEVD, the largest critical defect $\sqrt{a}_{c,n}$ expected in a volume V_n equal to $V_n = n \cdot V_{ref}$, being V_{ref} the so-called reference volume, can be computed as follows:

$$\sqrt{a}_{c,n} = \mu_{\sqrt{a}} + \sigma_{\sqrt{a}} \cdot (-ln(-ln(F)) + ln(n)) \quad (3)$$

being $\mu_{\sqrt{a}}$, $\sigma_{\sqrt{a}}$ the location and the scale parameter of the LEVD distribution and F the probability of the defect size of interest. $\mu_{\sqrt{a}}$, $\sigma_{\sqrt{a}}$ can be estimated with different techniques (e.g., through defect sampling on polished sections) and V_{ref} commonly represents the volume considered for the estimation.

Therefore, the maximum principal stress s_{max} of Equation 1 can be calculated from Equations 2 and 3 as [28]:

$$s_{max} = \frac{2 \cdot s_l}{1 - R} \quad (4)$$

where for the computation of $\sqrt{a}_{c,n}$ the final volume V_{opt} is considered, i.e., $V_n = V_{opt}$.

It must be noted that the limit stress can be also the fatigue strength at a given number of cycles to failure, computed with models available in the literature (e.g, [29–31]), which describe the high cycle fatigue regime, the very high cycle fatigue regime and the transition between the two. In this perspective, the methodology can be adopted for a wide range of life cycles. However, the P-S-N curves and their dependency on the defect size and on the tested volume must be experimentally assessed and this requires a quite larger number of time-consuming and expensive experimental tests. Moreover, it is also worth noting that, with the *TopFat* methodology, the information on the defect location and distribution is lost, whereas it is instead available with a micro-CT scan of the final components. Therefore, the main assumption is that each element contains the largest defect computed with Equation 3 and expected in the component volume. This represents a conservative

assumption, but allows to simplify the TO process. Moreover, no distinction between surface and internal defects is made with this approach. According to [20], the C_1 coefficient is equal to 1.41 in case of surface defects and to 1.56 in case of internal defects. For this reason, the C_1 coefficient is set to 1.41, i.e. by conservatively considering all the defects within the loaded volume as surface defects. The smaller accuracy in mapping the defect location, which is the main strength of the approach based on micro-CT inspections, is compensated by the advantage of taking into consideration the influence of defects directly in the TO process.

Finally, according to Equation 3, the volume V_n must be necessarily known to estimate the $\sqrt{a}_{c,n}$ value. If a volume constraint is set during the TO, V_n is known and corresponds to the volume of the optimized component. On the other hand, if no volume constraints are set, e.g., if the mass minimization is set as the objective of the optimization, the volume V_n to be considered in Equation 3 is not known before the optimization process and the *TopFat* methodology cannot be applied. In the following Section, the procedure developed to apply the *TopFat* methodology even if volume constraints are not set is described.

2.2 General methodology for the *TopFat* methodology with no volume constraints

As highlighted in Section 2.1, the proper application of the *TopFat* methodology requires that the volume of the component after the optimization (i.e., V_n in Equation 3) is known, in order to compute the limit stress for the first principal stress. This prevents the use of this methodology when volume constraints are not set. In order to overcome this shortcoming, an iterative procedure has been developed. The flowchart of the proposed methodology is shown in Figure 3. In the Figure, V_0 is the initial volume of the component, V_n the volume to consider in Equation 3 and V_{opt} is the volume of the component after the topology optimization process.

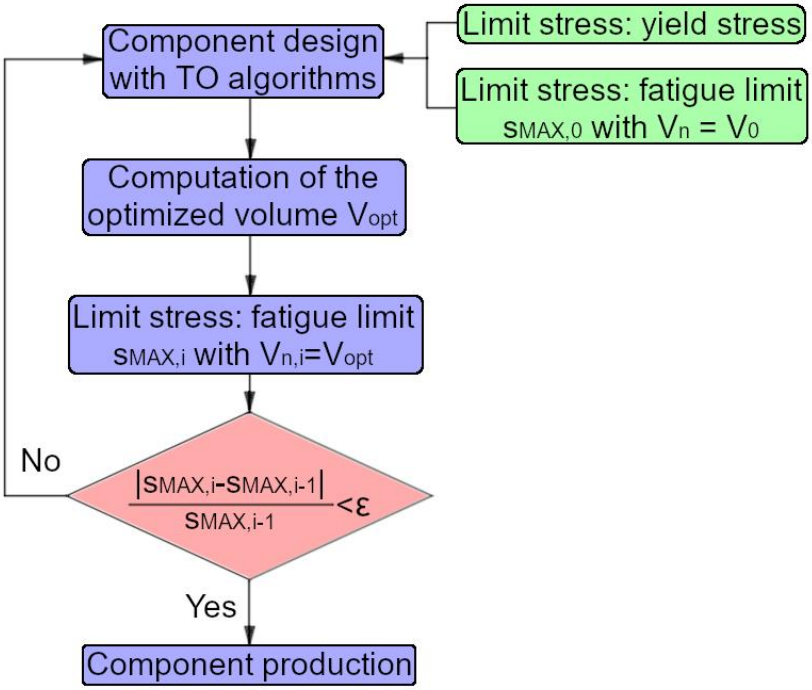

Figure 3. Flow chart of the methodology developed for the implementation of the *TopFat* methodology with no volume constraints.

According to Figure 3, the developed methodology involves repeated TOs, which are formulated as:

$$\begin{aligned} & \min_{\bar{\rho}} \ m(\bar{\rho}) \\ \text{such that} \quad & \frac{s_{eq}}{s_{adm}} - 1 \leq 0 \\ & \frac{s_1}{s_{max}} - 1 \leq 0 \\ \text{where} \quad & \rho_{inf} \leq \rho_e \leq 1 \\ \text{governed by} \quad & \bar{\rho} = \{\rho_1, \rho_2, \dots, \rho_{N_e}\} \\ & \bar{\bar{K}}(\bar{\rho})\bar{u} = \bar{F} \end{aligned} \tag{5}$$

where the mass m is minimized and only the equivalent stress s_{eq} and the maximum principal stress s_1 of each element are constrained. The maximum allowable principal stress s_{max} is computed according to Equations 2, 3 and 4. As the volume of the component after the optimization is not known, the volume of the initial component is at first assumed, i.e., $V_n = V_0$, and the maximum allowable principal stress $s_{max,0}$ accordingly calculated. Thereafter the topology optimization is run, with the software providing in output a map of the element relative densities. According to [9], the elements with relative density equal to 0 should be removed, since not necessary to withstand the applied load. On the contrary, the elements with relative density equal to 1 should be kept since fundamental to withstand the applied load. However, in order to assess the solution of the optimization process, the relative density varies continuously between 0 and 1 (e.g., with the SIMP method). This means that elements with intermediate densities are present in the final topology. The designer must choose if the elements with intermediate densities are to be considered or are to be excluded. In the developed procedure, the volume after the TO is computed as the volume of the elements with relative density above a threshold of 0.4. This represents a reasonable choice in practical applications, but the threshold level can be varied depending on the application. Further, in the present study, at the end of the optimization process, once only the elements with a relative density higher than 0.4 were kept, a FE analysis has been performed in order to verify the structural safety of the final topology.

Moreover, only elements with a positive first principal stress have been considered for the computation of the volume V_{opt}. It is here assumed a loading condition with stress ratio equal to 0. Once V_{opt} has been identified and following the scheme in Figure 3, an updated maximum first principal stress $s_{max,i}$ can be computed from Equations 2, 3 and 4 with $V_{n,i} = V_{opt}$. If the difference between the updated fatigue limit and that used in the TO is smaller than an ε value arbitrarily chosen, the procedure is concluded and the topology of the component is found. Indeed, when the convergence condition is met, the volume of the component in a subsequent TO would slightly reduce, thus with limited variations of the fatigue limit and changes of the final topology. On the contrary, if the convergence criterion is not satisfied, a second TO is run with the updated maximum first principal stress $s_{max,i}$. The procedure thus iteratively proceeds until the convergence criterion is met.

The convergence criterion could be equivalently defined from the volumes obtained at the end of an iteration and the preceding one. However, it must be noted that in this case the ε value for the convergence condition should be chosen depending on the material sensitivity to size-effect. If

the material shows a strong sensitivity to size-effect, the ε value should be smaller than that for materials for which the defect variation with the volume is limited. Rather, a convergence criterion based on the maximum allowable first principal stress yet retains the material sensitivity to the size-effect.

The proposed methodology can be applied when volume constraints are not set, thus when the final volume of the components cannot be assumed before the optimization process. However, this procedure can be employed also when volume constraints are set. For example, if the objective of the topology optimization is the maximization of the stiffness with a volume constraint (e.g., the 30% of the total volume), the volume of the optimized component includes elements with both positive and negative principal stresses. With the proposed general methodology, the real volume subjected to tensile loads and therefore at risk of crack nucleation can be taken into account, rather than the volume of the final component. Moreover, this procedure is also appropriate if the volume that experiences a defined stress amplitude is considered in place of the volume of the optimized component (e.g., the V_{90} defined in [23], corresponding to the volume above the 90% of the maximum applied stress). In this case, the volume V_{opt} to be considered corresponds to the sum of the elements with a relative density above the selected threshold, and with stress above the 90% of the maximum applied stress.

3. Engineering example – Aerospace bracket component

In this Section, the proposed methodology is applied to design an actual aerospace bracket. In [28], the *TopFat* procedure has been extended to *Hypermesh* commercial software, enabling its use by industrial designers for real-world applications. In Section 3.1, the model is described, while in Section 3.2 the structural-mechanical problems are presented. In particular, the TO design is performed with four different formulations: in the first formulation, the TO is performed without assuming a fatigue constraint, as shown in Figure 2; in the second formulation, a defect-free maximum allowable stress is considered; in the third, a TO with volume constraint, as in the original formulation of the *TopFat* algorithm (see Equation 1), is considered. Finally, the generalized TopFat procedure without volume constraints is adopted. In Section 3.3, the results of the four TO designs of the aerospace bracket are compared and discussed, highlighting the strength and limitations of the proposed methodology.

3.1 Mechanical model

Figure 4a shows the bracket, originally designed by *Leonardo Spa* within the Research Project AMICO for connecting the hatboxes in the cabin to the structural beams of an aircraft fuselage, while Figure 4b shows the division in non-design domain (NDD) in red and design domain (DD) in grey of the bracket for the TO process.

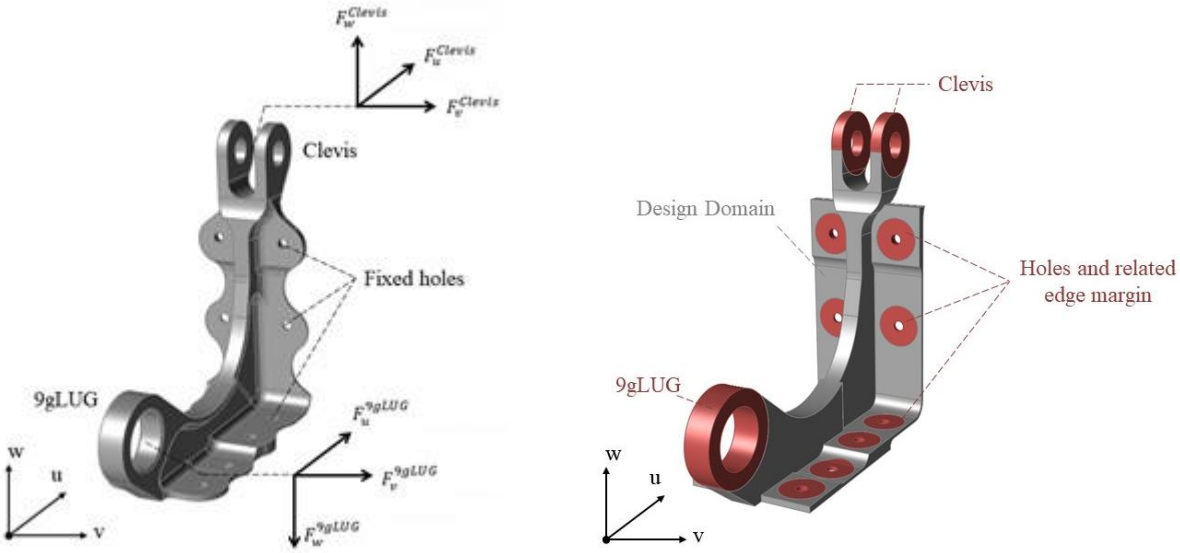

(a) (b)

Figure 4. Aerospace bracket: (a) original geometry and applied loads; (b) design and non-design domain zones

The hatboxes are mounted on the bracket through two pins, one in correspondence of the *Clevis* bushing and one in correspondence of the *9gLug* bushing. The bracket is fixed to the fuselage through 12 rivets, in correspondence of the *fixed holes* in Fig. 4a. As it can be noticed in Figure 4b, both the bushings, *Clevis* and *9gLug,* are set as NDD to ensure the connectivity with the pins. With similar considerations, an offset circular non-domain zone is set around the fixed holes. The DD is set equal to the remaining part of the bracket where the lightening features from the traditional manufacturing are removed. In particular, the full thickness of the rib is included and handles around the fixed holes are removed.

For the linear static FE analysis, the bracket has been discretized in 449444 first-order R-tetra elements, with maximum element size equal to 1 mm. The connection between the NDD and the DD is ensured using contact elements.

Regarding the boundary conditions, the rivets connections are simulated locking all the degrees of freedom of the internal hole surfaces whereas the pins are substituted by rigid elements (RBE2 in *Hypermesh*) to transfer the single point loads presented in Figure 4a to the internal surfaces of the bushings. In particular, the most severe conditions for the bracket are encountered during the acceleration manoeuvres with the hatboxes fulfilled with passengers goods. Under these most severe conditions, it is possible to evaluate the pin loads transferred to the bracket with respect to the reference system called *u-v-w* reported in Fig. 4a. For the fatigue regime, the nominal load conditions are calculated by dividing the maximum ones by a factor equal to 1.5. As the loads refer to the acceleration phase, it seems reasonable to assume that the loading case is a case $R = 0$. However, it is worth noticing that the proposed methodology is not limited to the case R=0 and that, according to Equation 4, the lower R, the lower the maximum allowable principal stress s_{max}. Table 1 reports the maximum and the nominal conditions which the brackets undergo during its life, as calculated by *Leonardo Spa* from a full aircraft model analysis.

Load	Worst condition	Nominal condition
F_w^{Clevis} $[N]$	10432	6955

$F_u^{Clevis}\ [N]$	12	8
$F_v^{Clevis}\ [N]$	1121	747
$F_w^{9gLUG}\ [N]$	-6861	-4574
$F_u^{9gLUG}\ [N]$	21830	14553
$F_v^{9gLUG}\ [N]$	1372	915

Table 1. Applied loads in worst and nominal conditions

Hypermesh allows accounting for both the loading conditions by defining two different Load Step identities. As the load amplitudes of the static and fatigue conditions are different, at each iteration of the optimization process, two linear static analyses are performed, one with the maximum loading conditions, i.e., those for the static verification, and one with the nominal loading conditions, which are instead assumed for the fatigue regime.

No safety factor has been retained for both the static and fatigue loading conditions. Nevertheless, the discussion on the proposed methodology is still valid, as the adoption of a safety factor would equally decrease the maximum allowable first principal stress for all the retained optimization formulations.

The original component was made of Aluminium T7075 and manufactured by milling a semifinished product. The original weight of the component was 160 g. According to the specifications of *Leonardo Spa*, the new bracket is to be manufactured by Electron Beam Melting (EBM) additive process with Ti6Al4V powder by *Arcam* company. The material data of the EBM Ti6Al4V are reported in Table 2 together with the data related to the defect distribution required by Equation 3.

Parameter	Value
EBM Ti6Al4V Young modulus $E\ [\ GPa]$	119
EBM Ti6Al4V Poisson ratio ν	0.3
EBM Ti6Al4V density $\rho\ [g/mm^3]$	$4.42 \cdot 10^{-3}$
EBM Ti6Al4V Yield limit $R_{p02}[\ MPa]$	866
EBM Ti6Al4V Ultimate strength $R_m[\ MPa]$	930
EBM Ti6Al4V Vickers hardness HV	350
Superficial defect location parameters C_1	1.41
LEVD location parameter $\mu_{\sqrt{a}}\ [\mu m]$	60.78
LEVD scale location parameter $\sigma_{\sqrt{a}}[\mu m]$	60.15
Reference volume $V_0[mm^3]$	5000

Table 2. Material data and defect population parameters

The defect population data, $\mu_{\sqrt{a}}$ and $\sigma_{\sqrt{a}}$, are representative and close to those extrapolated in [32] where *Arcam* EBM Ti6Al4V samples have been tested. It can be assumed that the analysed component will be produced with similar process parameters. Therefore, the retained LEVD parameters, $\mu_{\sqrt{a}}$ and $\sigma_{\sqrt{a}}$, can be assumed to be fairly close to those characterizing the final component. If very different process parameters or post-production treatments, such as the hot isostatic pressure (HIP), were employed, a novel defect analysis would be necessary to estimate the LEVD parameters as indicated by [23]. Generally speaking, the LEVD parameters can be determined

through a micro-CT of the specimens or through metallography analysis of the fracture surface [12,22].

3.2 Structural-mechanical problem

According to the generalized *TopFat* procedure described in Section 2.2, the goal of the TO process is to minimize the mass of the component while guaranteeing the structural safety against both static and fatigue loads. The optimization problem is thus formulated as

$$\begin{aligned} \text{while} \quad & \frac{\left|s_{max,i} - s_{max,i-1}\right|}{s_{max,i-1}} < \varepsilon \\ & \min_{\bar{\rho}} \; m(\bar{\rho}) \\ \text{such that} \quad & \frac{s_{eq}}{s_{adm}} - 1 \leq 0 \\ & \frac{s_1}{s_{max,i-1}} - 1 \leq 0 \\ \text{where} \quad & \rho_{inf} \leq \rho_e \leq 1 \\ \text{governed by} \quad & \bar{\rho} = \{\rho_1, \rho_2, \dots, \rho_{N_e}\} \\ & \bar{\bar{K}}(\bar{\rho})\bar{u} = \bar{F} \end{aligned} \tag{6}$$

where the equivalent stress s_{eq} is calculated for each element according to the Von Mises criterion, the maximum allowable stress s_{adm} is set equal to the Yield limit of the material, i.e., 866 MPa, and maximum first principal stress $s_{max,i-1}$ is evaluated according to the procedure described in Section 2.2. At the beginning of the TO, the initial volume of the component V_0 is 74700 mm^3, which corresponds to a maximum allowable first principal stress $s_{max,0}$ of 440 MPa. According to the iterative procedure of Section 2.2, the $s_{max,i-1}$ value is updated in accordance with the optimized volume until the convergence criterion is met. Here, the ε value has been set equal to 1%, i.e., the iterative procedure stops when the discrepancy between the maximum allowable stresses calculated in two consecutive iterations is smaller than 1%.

In order to investigate strength and limitations, results of the proposed methodology are compared to those obtained with TO formulations proposed in the literature. In particular, following the scheme of Figure 2, a first TO is performed without imposing a fatigue constraint. The formulation of this TO problem can be written as

$$\begin{aligned} & \min_{\bar{\rho}} m(\bar{\rho}) \\ \text{such that} \quad & \frac{s_{eq}}{s_{adm}} - 1 \leq 0 \\ & \rho_{inf} \leq \rho_e \leq 1 \\ \text{where} \quad & \bar{\rho} = \{\rho_1, \rho_2, \dots, \rho_{N_e}\} \\ \text{governed by} \quad & \bar{\bar{K}}(\bar{\rho})\bar{u} = \bar{F} \end{aligned} \tag{7}$$

where the maximum allowable stress s_{adm} is set equal to the yield limit of the material reported in Table 2. Accordingly, only the static loading conditions are considered in *Hypermesh*.

The second formulation accounts for a fatigue strength that is independent from the defect size. The TO formulation is the same reported in Equation 6, where the mass is minimized, and the

constraints are imposed for both the static and fatigue conditions. In particular, the maximum first principal stress s_{max} is assumed as $1.6 \cdot HV$, that is 560 MPa and is the ideal fatigue strength according to [23].

Finally, the bracket is optimized by minimizing its compliance and assuming a volume reduction constraint also used to calculate the maximum allowable first principal stress. In particular, the optimization problem is formulated as

$$\begin{aligned} & \min_{\bar{\rho}} \; C(\bar{\rho}) \\ \text{such that} \quad & \frac{V}{V_{opt}} - 1 \leq 0 \\ & \frac{s_{eq}}{s_{adm}} - 1 \leq 0 \\ & \frac{s_1}{s_{max}} - 1 \leq 0 \\ & \rho_{inf} \leq \rho_e \leq 1 \\ \text{where} \quad & \bar{\rho} = \{\rho_1, \rho_2, \dots, \rho_{N_e}\} \\ \text{governed by} \quad & \bar{\bar{K}}(\bar{\rho})\bar{u} = \bar{F} \end{aligned} \tag{8}$$

where the final volume V_{opt} is set equal to 50000 mm^3, which corresponds to a reduction of one third with respect to the initial volume V_0 and to a maximum allowable first principal stress s_{max} of 450 MPa.

In all the described optimizations, a symmetry constraint has been adopted, which guarantees the symmetry of the component with respect to the middle plane defined by the directions *u*-*w* of Figure 4.

3.3 Results

The TOs are performed within the *Hypermesh* environment, which adopts an algorithm based on the dual method [33]. In all the cases, the TO process reaches a feasible solution with respect to the imposed constraints. Table 3 summarizes the obtained results for each formulation.

Formulation	$\boldsymbol{m}$ **[g]**	**Mass reduction** $\frac{\mathbf{160} - \boldsymbol{m}}{\mathbf{160}}$	$\boldsymbol{s_{1,max}}$ $(\boldsymbol{s_{max}})$ **[MPa]**	**Number of elements for** $\boldsymbol{s_1}$ **> 400 MPa**	$\boldsymbol{s_{eq,max}}$ $(\boldsymbol{s_{adm}})$ **[MPa]**	**Iterations**
TopFat iterative	133.4	16.6%	489.7 (490)	136	780.6 (866)	75+62+94
TopFat with Volume Constraint	157.0	1.9%	449.7 (450)	16	555.7 (866)	74
Free-defect fatigue constraint	123.7	22.7%	559.9 (492)	337	857.8 (866)	101
No fatigue constraint	119.3	25.4%	1499.6 (494)	5273	865.2 (866)	89

Table 3. Results of the TO with the retained formulations

As shown in Table 3, with all the formulations, consistent mass saving can be achieved with respect to the original component made in Aluminium. The *TopFat* procedure is able to achieve the real optimum of the structure which guarantees the structural safety of the component with respect to both the static and fatigue loading conditions, as can be appreciated by comparing the maximum stress calculated in the component and the corresponding limit value reported in brackets. In particular, the limit value s_{max} has been calculated by considering the defect population data in Table 2 and the resulting volume. Regarding the optimization with only the yield stress constraint, in accordance with the flowchart of Figure 2, a FE analysis of the obtained topology has been performed with the nominal loading conditions. The first principal stress is almost equal to 1000 MPa in the most loaded elements which is far beyond the limit of fatigue for the resulting volume (10345 mm^3), that is 494 MPa, and also beyond the fatigue limit in case of a defect-free material, that is 560 MPa. In the case of the defect-free constraint optimization, the limit of fatigue for the resulting volume (11727 mm^3) is equal to 492 MPa, which is consistently lower than the maximum first principal stress experienced by the component (559 MPa). Therefore, from a structural point of view, these solutions are not feasible.

Further, the use of a volume constraint limits the achievable reduction of mass. Instead, in the proposed approach, the topology is iteratively refined, thus maximizing the mass reduction. In particular, in the present case, three iterations were necessary to satisfy the convergence criterion of Equation 6, with the maximum allowable first principal stress being equal to 490 MPa in the last iteration. The number of iterations depends on the material sensitivity to the defect size. In the present study, at the end of the first iteration, the final volume was 13865 mm^3 and the updated fatigue limit was 483 MPa. At the end of the second iteration the final volume was 11797 mm^3, which led to a fatigue limit of 490 MPa. As the convergence criterion was not yet satisfied, a third iteration was necessary. This led to a final volume of 11568 mm^3, for which the fatigue limit was 490.4 MPa. Being the difference between this fatigue limit and the one of the previous iteration smaller than 1% (0.08%), the convergence criterion is met. It can be indeed expected that a further optimization with the updated value of 490.4 MPa would have led to almost the same topology.

Regarding the computational time, all the formulations achieved the optimal results in about 100 iterations, taking almost 200s per iteration on a Desktop Server Machine with Intel Xeon E5-2640 and 64 GB of RAM. Due to the iterative procedure, the proposed methodology thus requires a higher computational effort, almost tripling the time with respect to the volume-constraint approach. Instead, when the fatigue constraint is not imposed or is assumed independent from the defect size, the structural safety is not guaranteed and a time-consuming trial-and-error approach might be necessary to achieve a feasible solution. As such, the effective computational effort of a fatigue-unconstrained TO or of a defect size independent formulation can be consistently high. The computational time of the proposed methodology could be consistently reduced by imposing that the maximum first principal stress varies at each iteration of the optimization process in accordance with the actual volume. In this case, the optimal topology would be found through one single optimization process, i.e., without the iterative procedure described in Section 2.2. However, the use of variable constraints within an optimization problem can be self-defeating [34].

Regarding the mass of the component, it can be noticed that the mass reduction obtained with the defect-free fatigue constraint is only 6% higher than that obtained with the proposed iterative methodology. However, with the proposed formulation, the feasibility of the optimal results is yet

guaranteed and does not require further verifications on the largest defect location. The major mass reduction of the defect-free constraint formulation is mainly due to the final topologies which are reported in Figure 5, with the first principal stress contour plots as resulting from a FE reanalysis. The contour plots are limited between 0 and 400 MPa in accordance with Table 3.

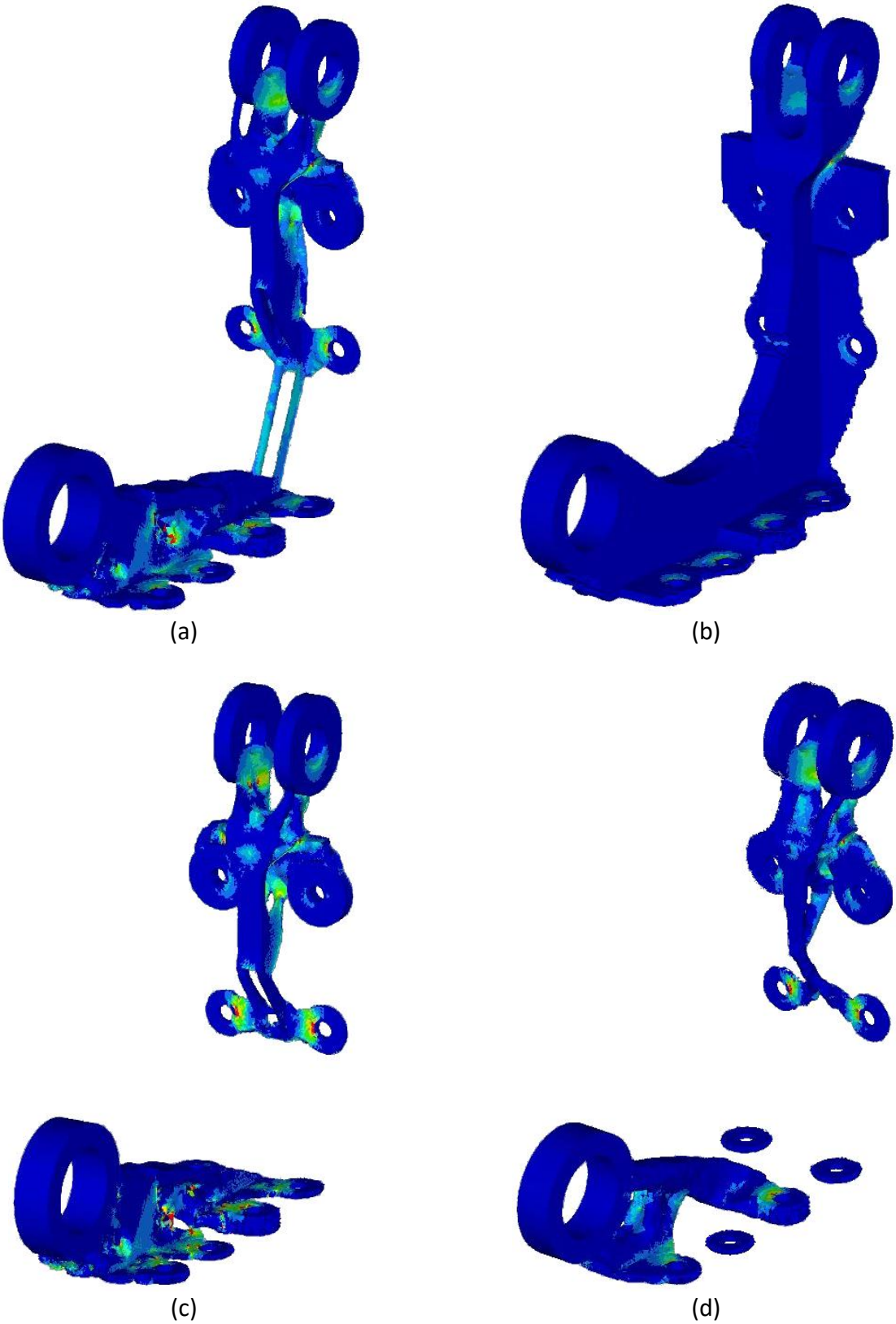

(a) (b)

(c) (d)

Figure 5. First principal stress contour plots of the optimal topologies according to the different formulations: (a) TopFat without volume constraints; (b) TopFat with volume constraints; (c) defect-free fatigue constraint; (d) no fatigue constraint

As shown in the Figure, the topologies are rather different from the others. In particular, when the fatigue constraint is not imposed or when the defect-free fatigue limit is assumed, the two bushings are separated, which explains the higher mass obtained with the *TopFat* procedure. With the *TopFat* methodology a mono-component is obtained, since the connecting tiny bars allow unloading the regions in correspondence of the bottom rivets of the upper part (Cf. Figure 5a and Figure 5c). Further, if the bracket has to be a mono-component, for example for mounting requirements, a further constraint must be retained in the topology optimization. For example, a non-design domain region can be locally defined. Accordingly, the discrepancy with respect to the mass obtained with the *TopFat* procedure would be smaller.

It is also worth highlighting that the proposed methodology assumes that the largest defect is equivalently present in each element of the FE model. This represents a conservative assumption, which allows simplifying the topology optimization process. Accordingly, the information on the defect location and distribution is lost, which is instead known with a micro-CT of the final component. In this regard, it is expected that further minimization of the component mass can be achieved. However, it is worth noticing that, for the studied component, the number of elements that experiences a first principal stress above 400 MPa (red elements in Figure 5) is rather limited, as shown in Figure 5 and reported in Table 3. As a consequence, the assumption for which the largest defect is present in correspondence of these highly stressed elements does not significantly affect the achievable mass reduction. On the contrary, the number of elements with a first principal stress above 400 MPa is consistently higher in the topologies obtained with the fatigue-unconstrained formulation and with the defect-free constraint formulation. As such, further doubts arise on the structural feasibility of these topologies.

4. Conclusions

In the present paper, a generalized formulation of the defect-driven topology optimization (TO) methodology for fatigue design, named *TopFat*, is presented. The methodology allows guaranteeing the structural safety against both static and fatigue loading conditions of additively manufactured (AM) components, while minimizing the mass. Defects resulting from AM processes, which are prone to nucleate cracks and affect the static and fatigue strength, are accounted for within the optimization formulation. In particular, the defect size distribution, modelled as a Largest Extreme Value Distribution (LEVD), is considered within the optimization problem, by imposing a constraint on the first principal stress, that causes the crack propagation. The methodology assumes that the largest defect is equivalently present in each element of the Finite Element (FE) model. This represents a conservative assumption, which allows simplifying the TO process, while the information on the defect location is lost. As the largest defect of the LEVD depends on the final volume of the component, which changes according to the topology, an iterative procedure is here proposed where the optimization problem is formulated without imposing volume constraints. The procedure is implemented in *Hypermesh* commercial software.

The application to an actual aerospace bracket component, originally designed by Leonardo Spa for the Research Project AMICO, has shown that considering the defect population induced by the Electron Beam Melting (EBM) additive process consistently affects the final topology and leads to a

feasible optimum. In comparison with other formulations, such as the fatigue-unconstrained optimization, the proposed methodology guarantees the structural safety of the component with respect to both the static and fatigue conditions. Further, even though the methodology conservatively assumes that the largest defect is equivalently present in each element, the mass reduction is very close to that achieved with a formulation with defect-free fatigue constraint. Therefore, the influence of the conservative assumption on the mass reduction is not significant for the considered component. Finally, results show that, with respect to a volume constraint formulation of *TopFat*, an additional 15% of mass saving can be achieved by adopting the proposed iterative procedure, in exchange for a tripled computational time. In this regard, it is worth noticing that, following the standard fatigue-unconstrained approaches, the computational effort required to obtain a feasible solution can be consistently high, as a time-consuming trial-and-error approach might be necessary.

In order to achieve further mass reduction, future work will address the conservative assumption that the largest defect is equivalently present in each element. For instance, as the fatigue strength has different values according to the location of the defect (mainly internal and external), the design domain can be divided in two parts, one retaining the external elements and one retaining the internal elements, while adopting different fatigue limits for the two.

Overall, the presented procedure can be employed for almost all industrial AM re-designs. It exploits the power and accessibility of commercial software to set up the optimisation, FE discretisation and analysis whereas no coding is needed to formulate the defect-driven TO for fatigue design.

Acknowledgments

This work has been supported by the Research Project AMICO (code ARS01_00758) funded by the Italian Ministry of Education, University and Research.

References

1. Frazier, W.E. Metal additive manufacturing: A review. *J. Mater. Eng. Perform.* **2014**, *23*, 1917–1928, doi:10.1007/s11665-014-0958-z.
2. Yakout, M.; Elbestawi, M.A.; Veldhuis, S.C. A review of metal additive manufacturing technologies. *Solid State Phenom.* **2018**, *278 SSP*, 1–14, doi:10.4028/www.scientific.net/SSP.278.1.
3. Gibson, I.; Rosen, D.; Stucker, B. *Additive Manufacturing Technologies*; Second Edi.; Springer, 2015; ISBN 9781493921126.
4. Plocher, J.; Panesar, A. Review on design and structural optimisation in additive manufacturing: Towards next-generation lightweight structures. *Mater. Des.* **2019**, *183*, 108164, doi:10.1016/J.MATDES.2019.108164.
5. Caivano, R.; Tridello, A.; Codegone, M.; Chiandussi, G. A new methodology for thermostructural topology optimization: Analytical definition and validation. *Proc. Inst. Mech. Eng. Part L J. Mater. Des. Appl.* **2021**, *235*, 481–500, doi:10.1177/1464420720970246.
6. Benedetti, M.; du Plessis, A.; Ritchie, R.O.; Dallago, M.; Razavi, S.M.J.; Berto, F. Architected cellular materials: A review on their mechanical properties towards fatigue-tolerant design and fabrication. *Mater. Sci. Eng. R Reports* **2021**, *144*, 100606, doi:10.1016/J.MSER.2021.100606.

7. Wu, W.; Hu, W.; Qian, G.; Liao, H.; Xu, X.; Berto, F. Mechanical design and multifunctional applications of chiral mechanical metamaterials: A review. *Mater. Des.* **2019**, *180*, 107950, doi:10.1016/J.MATDES.2019.107950.

8. Boursier Niutta, C.; Ciardiello, R.; Tridello, A. Experimental and Numerical Investigation of a Lattice Structure for Energy Absorption: Application to the Design of an Automotive Crash Absorber. *Polymers (Basel).* **2022**, *14*, 1116–1137, doi:https://doi.org/10.3390/polym14061116.

9. Bendsøe, M.P.; Sigmund, O. *Topology optimization*; Second Edi.; Springer, 2002;

10. Sigmund, O.; Maute, K. Topology optimization approaches: A comparative review. *Struct. Multidiscip. Optim.* **2013**, *48*, 1031–1055, doi:10.1007/s00158-013-0978-6.

11. Bendsøe, M.P.; Sigmund, O. Material interpolation schemes in topology optimization. *Arch. Appl. Mech.* **1999**, *69*, 635–654, doi:10.1007/s004190050248.

12. Tridello, A.; Fiocchi, J.; Biffi, C.A.; Chiandussi, G.; Rossetto, M.; Tuissi, A.; Paolino, D.S. Effect of microstructure, residual stresses and building orientation on the fatigue response up to 10^9 cycles of an SLM AlSi10Mg alloy. *Int. J. Fatigue* **2020**, *137*, 105659, doi:10.1016/j.ijfatigue.2020.105659.

13. Leuders, S.; Lieneke, T.; Lammers, S.; Tröster, T.; Niendorf, T. On the fatigue properties of metals manufactured by selective laser melting - The role of ductility. *J. Mater. Res.* **2014**, *29*, 1911–1919, doi:10.1557/jmr.2014.157.

14. Ronchei, C.; Vantadori, S.; Carpinteri, A. Fatigue lifetime assessment of AM metallic components according to a strain-based criterion. *Int. J. Fatigue* **2022**, *156*, 106674, doi:10.1016/J.IJFATIGUE.2021.106674.

15. Romano, S.; Brückner-Foit, A.; Brandão, A.; Gumpinger, J.; Ghidini, T.; Beretta, S. Fatigue properties of AlSi10Mg obtained by additive manufacturing: Defect-based modelling and prediction of fatigue strength. *Eng. Fract. Mech.* **2018**, *187*, 165–189, doi:10.1016/j.engfracmech.2017.11.002.

16. Sanaei, N.; Fatemi, A. Defects in additive manufactured metals and their effect on fatigue performance: A state-of-the-art review. *Prog. Mater. Sci.* 2021, *117*, 100724.

17. Beretta, S.; Romano, S. A comparison of fatigue strength sensitivity to defects for materials manufactured by AM or traditional processes. *Int. J. Fatigue* **2017**, *94*, 178–191, doi:10.1016/j.ijfatigue.2016.06.020.

18. Masuo, H.; Tanaka, Y.; Morokoshi, S.; Yagura, H.; Uchida, T.; Yamamoto, Y.; Murakami, Y. Influence of defects, surface roughness and HIP on the fatigue strength of Ti-6Al-4V manufactured by additive manufacturing. *Int. J. Fatigue* **2018**, *117*, 163–179, doi:10.1016/j.ijfatigue.2018.07.020.

19. Solberg, K.; Guan, S.; Razavi, S.M.J.; Welo, T.; Chan, K.C.; Berto, F. Fatigue of additively manufactured 316L stainless steel: The influence of porosity and surface roughness. *Fatigue Fract. Eng. Mater. Struct.* **2019**, *42*, 2043–2052, doi:10.1111/ffe.13077.

20. Yamashita, Y.; Murakami, T.; Mihara, R.; Okada, M.; Murakami, Y. Defect Analysis and Fatigue Design Basis for Ni-based Superalloy 718 manufactured by Additive Manufacturing. In Proceedings of the Procedia Structural Integrity; Elsevier B.V., 2017; Vol. 7, pp. 11–18.

21. du Plessis, A.; Yadroitsava, I.; Yadroitsev, I. Effects of defects on mechanical properties in metal additive manufacturing: A review focusing on X-ray tomography insights. *Mater. Des.*

2020, *187*, 108385, doi:10.1016/j.matdes.2019.108385.

22. Romano, S.; Abel, A.; Gumpinger, J.; Brandão, A.D.; Beretta, S. Quality control of AlSi10Mg produced by SLM: Metallography versus CT scans for critical defect size assessment. *Addit. Manuf.* **2019**, *28*, 394–405, doi:10.1016/j.addma.2019.05.017.
23. Murakami, Y. *Metal Fatigue: Effects of Small Defects and Nonmetallic Inclusions*; Elsevier Ltd, 2002; ISBN 9780128138779.
24. Murakami, Y. Inclusion rating by statistics of extreme values and its application to fatigue strength prediction and quality control of materials. *J. Res. Natl. Inst. Stand. Technol.* **1994**, *99*, 345, doi:10.6028/jres.099.032.
25. Beretta, S. More than 25 years of extreme value statistics for defects: Fundamentals, historical developments, recent applications. *Int. J. Fatigue* **2021**, *151*, 106407, doi:10.1016/J.IJFATIGUE.2021.106407.
26. Romano, S.; Miccoli, S.; Beretta, S. A new FE post-processor for probabilistic fatigue assessment in the presence of defects and its application to AM parts. *Int. J. Fatigue* **2019**, *125*, 324–341, doi:10.1016/j.ijfatigue.2019.04.008.
27. Gao, X.; Caivano, R.; Tridello, A.; Chiandussi, G.; Ma, H.; Paolino, D.; Berto, F. Innovative formulation for topological fatigue optimisation based on material defects distribution and TopFat algorithm. *Int. J. Fatigue* **2021**, *147*, 106176, doi:10.1016/J.IJFATIGUE.2021.106176.
28. Caivano, R.; Tridello, A.; Barletta, G.; Gallo, N.; Baroni, A.; Berto, F.; Paolino, D. Defect-Driven Topology Optimisation: TopFat algorithm validation via 3D components re-design for real industrial applications. *Procedia Struct. Integr.* **2022**, *39*, 81–88, doi:10.1016/J.PROSTR.2022.03.075.
29. Matsunaga, H.; Sun, C.; Hong, Y.; Murakami, Y. Dominant factors for very-high-cycle fatigue of high-strength steels and a new design method for components. *Fatigue Fract. Eng. Mater. Struct.* **2015**, *38*, 1274–1284, doi:10.1111/ffe.12331.
30. Paolino, D.S.; Tridello, A.; Chiandussi, G.; Rossetto, M. S-N curves in the very-high-cycle fatigue regime: statistical modeling based on the hydrogen embrittlement consideration. *Fatigue Fract. Eng. Mater. Struct.* **2016**, *39*, doi:10.1111/ffe.12431.
31. Tridello, A.; Boursier Niutta, C.; Rossetto, M.; Berto, F.; Paolino, D.S. Statistical models for estimating the fatigue life, the stress–life relation, and the P-S–N curves of metallic materials in Very High Cycle Fatigue: A review. *Fatigue Fract. Eng. Mater. Struct.* **2022**, *45*, 332–370, doi:10.1111/ffe.13610.
32. Niu, M.C. *Airframe Stress Analysis and Sizing*; Second Edi.; 1999; ISBN 978-9627128120.
33. AltairEngineering https://support.altair.com/csm?id=altair_product_documentation.
34. Boursier Niutta, C.; Wehrle, E.J.; Duddeck, F.; Belingardi, G. Surrogate modeling in design optimization of structures with discontinuous responses: A new approach for ill-posed problems in crashworthiness design. *Struct. Multidiscip. Optim.* **2018**, *57*, 1857–1869, doi:10.1007/s00158-018-1958-7.